Optoelectronic and thermodynamic properties of the Yttrium filled skutterudite YFe_4P_{12}

S. Ilhem Messaoudi*, A. Touia*, and O. Addou

Materials Science and Applications Laboratory, Faculty of Sciences and Technology, University of Ain Temouchent, Belhadj Bouchaib. BP 284, Ain-Temouchent, 46000, Algeria.
*e-mail: *amina.touia@univ-temouchent.edu.dz; *ilhem.messaoudi@univ-temouchent.edu.dz.*

Received 28 September 2023; accepted 3 May 2024

In this work, we sought to understand the structural, electronic, optical, and thermodynamic properties of YFe_4P_{12} compound using the full-potential and linear augmented plane-wave method (FP-LAPW) based on density functional theory (DFT). Our calculation of the lattice parameter of this compound YFe_4P_{12} is reasonably in good agreement with the experimental results. Calculations carried out on the electronic band structure showed that the YFe_4P_{12} compound is classified as a direct-gap half-metal in the minority spins. Moreover, optical properties, such as the optical absorption coefficient, real and imaginary parts of the dielectric function, optical conductivity, refractive index, and optical reflectivity have been studied. The effects of pressure and temperature on the lattice parameter, heat capacities, coefficients of thermal expansion, entropy, and Debye temperature were explored using the quasi-harmonic Debye model.

Keywords: YFe_4P_{12}; optical; thermodynamic; FP-LAPW; Wien2k.

DOI: https://doi.org/10.31349/RevMexFis.70.061601

1. Introduction

The physical properties of filled skutterudites at low temperatures are of considerable interest to researchers. Indeed, a wide variety of magnetic and electronic states can be demonstrated in these compounds, including magnetic order [1, 2] and superconductors [3, 4]. Jietschko and Braun [5] showed in 1977 that it is possible to insert rare earth in the 2a site of the binary Skutterudites (between the octahedron $TrPn_6$ to form a ternary Skutterudites of the "filled Skutterudites" type of formula $RETr_4Pn_2$ (RE= Y, La, Ce, Pr, Nd, Sm, Tm, Eu, Gd, Tb, Yb, U, Th; Tr = Fe, Ru, Os and Pn = P, As, Sb). This filling of the empty cage is made possible by the concomitant substitution of the transition metal by an element with one less electron (Iron, Ruthenium, or Osmium) to compensate for the electrons brought by the electropositive ion. Since then, it has been shown that many other elements can be inserted into the structure, including alkaline earth [6, 7] thorium [8] uranium [9], sodium or potassium [10], and thallium [11]. The insertion of these electropositive ions can lead to excellent thermoelectric properties at high temperatures [12]. Skutterudites have become an illustration of the recently developed model of Phonon-Glass Electron-Crystal (PGEC), which can, in principle, lead to the development of new thermoelectric materials. Other phenomena such as hybridization gap semiconductor (HGS), heavy fermion metal (HFM), field-induced heavy fermion metal (FIHF), and non-Fermi-liquid (NFL) make filled skutterudites the most commonly used thermoelectric materials [13]. Skutterudites in general and filled or partially filled skutterudites in particular have recently become a hot topic, due to their physical behaviors being sensitive to changes in their fillings and to changes in temperature and pressure [14]. A large number of studies show that they possess fascinating properties such as optical, thermodynamic, and magnetic properties. Filled skutterudites have attracted the attention of researchers for several years, which has increased the number of syntheses and, therefore, expanded their uses in several application areas. Fe-filled skutterudites have been the subject of several studies that have shown that these materials possess significant optical and thermodynamic electronic properties. In addition to their many known properties such as magnetism and superconducting [15, 16] behaviors as well as the metal-insulator transition, which justifies that skutterudites are among the most studied and exploited in their family. This work focuses on the study of the skutterudite alloy YFe_4P_{12}, which has interesting optoelectronic and thermodynamic properties.

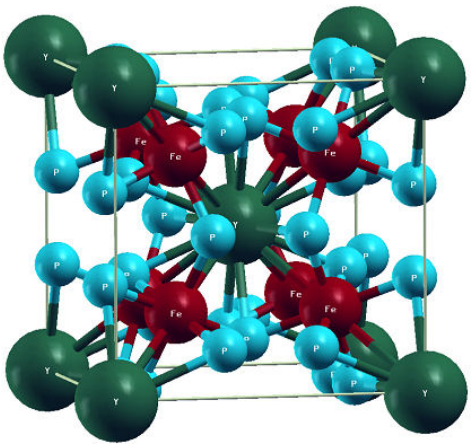

FIGURE 1. Crystal structure of YFe_4P_{12}.

TABLE I. Lattice constant a_0 (in Å), bulk modulus B (in GPa), its pressure derivative B' and minimum energy at equilibrium E_0 (in Ry) using GGA (PBE) for both states, non-magnetic state (NM) and ferromagnetic state (FM) at $T = 0$ K and $P = 0$ GPa.

YFe_4P_{12}						
Pres.Cal	a_0(Å)	y	z	B(GPa)	B'	E_0(Ry)
NM-GGA-PBE	7.8327	0.353	0.1501	188.4807	8.5806	-25165.1023
FM-GGA-PBE	7.8226	0.353	0.1501	164.0651	6.3822	-25164.9887
Exp.	7.7896[a]	-	-	-	-	-
	7.789[b]	-	-	144[b]	-	-
	7.7913[c]	-	-	-	-	-

[a]Ref. [22], [b]Ref. [24], [c]Ref. [25].

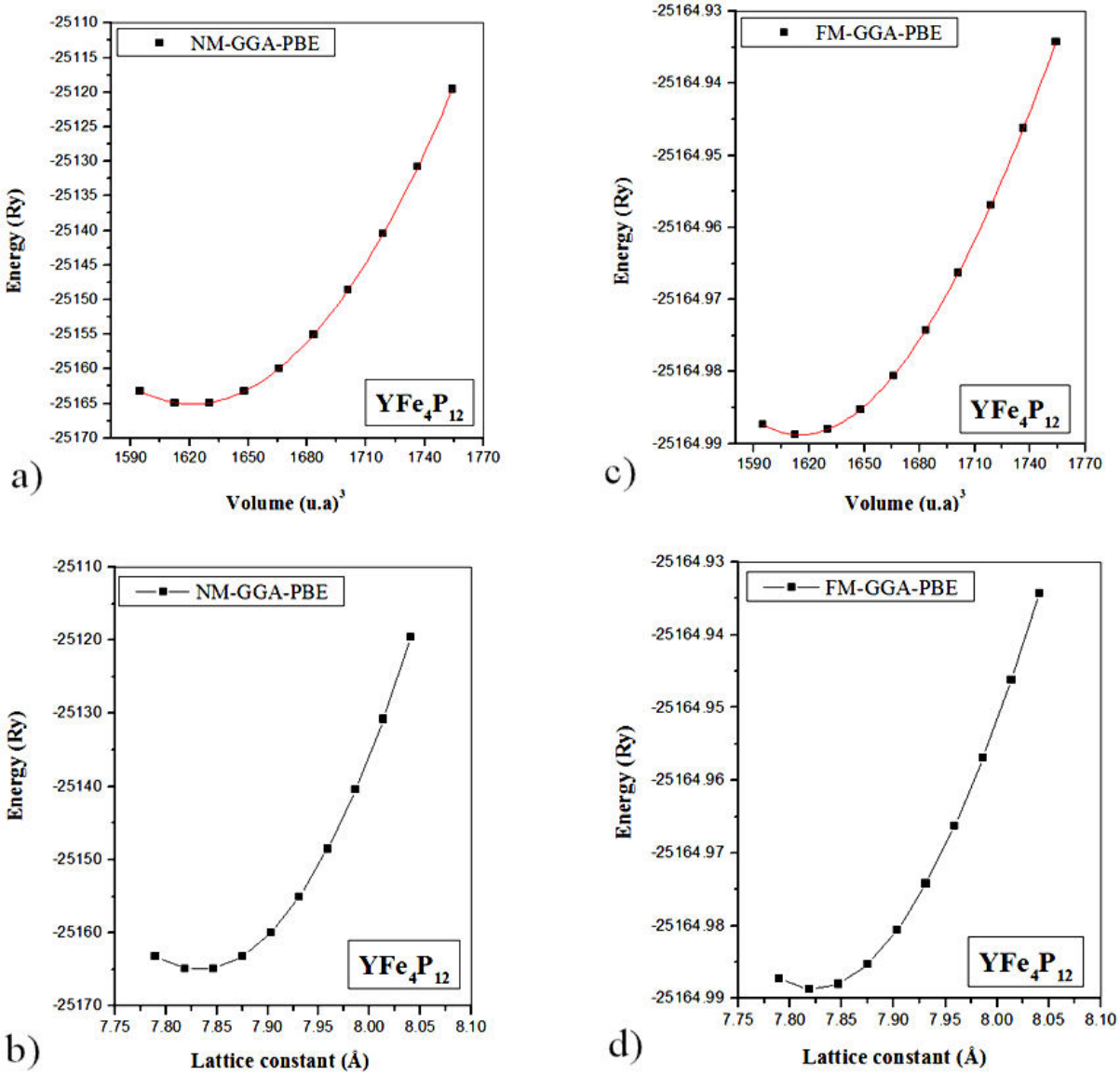

FIGURE 2. The total energies for both non-magnetic (NM) and ferromagnetic (FM) configurations with the GGA-PBE approximation as a function of volume and lattice constant.

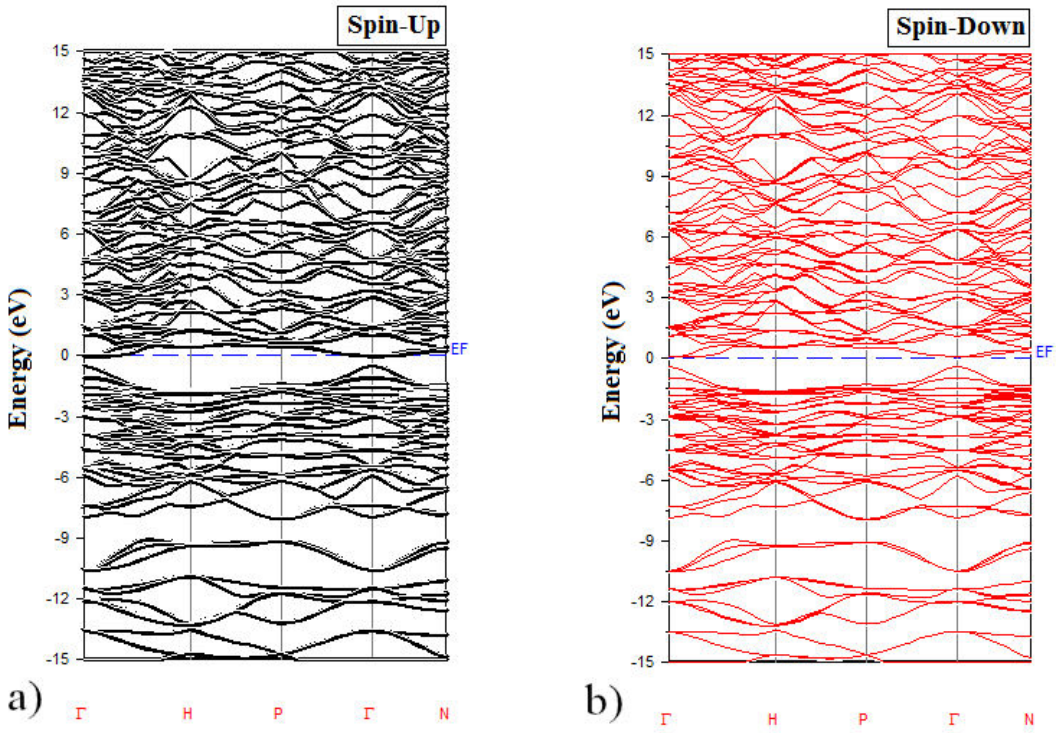

FIGURE 3. The band structure of YFe_4P_{12} at the equilibrium structure using GGA-PBE approximation with spin polarization.

2. Computational details

The calculations were performed using the wien2k code [17]. The code made it possible to calculate the density of states and the total energy of the crystal. This process is based on the density functional theory DFT [18]. We treated the term exchange and correlation using the GGA-PBE (Perdew, Burke, and Ernzerhof) [19] for the both non-magnetic (NM) and ferromagnetic (FM) states. The basic functions, electronic density, and potentials were developed in spherical harmonics up to $l_{\max} = 10$ to obtain the convergence of the eigenvalues, while the charge density was extended up to $G_{\max} = 12$. However, in the interstitial region, these functions are considered extended plane waves and are developed in the Fourier series with a cutoff parameter $R; MT \times K_{\max} = 9$, which presents a good compromise between calculation accuracy and reasonable execution time. The integration in the reciprocal space was carried out with a mesh of $14 \times 14 \times 14$, giving rise to 5000 points k in the irreducible Brillouin zone (IBZ) [20], which is sufficient to achieve convergence. For this prediction, we chose muffin-tin radii (R_{MT}) equal to 2.5, 2.37, and 1.85 for the three atoms Y, Fe, and P, respectively.

3. Results and discussion

3.1. Structural properties

In this section, we are interested in structural determination, which is the first important step in understanding materials from a microscopic point of view. We used the FP-LAPW method to study the skutterudite alloy YFe_4P_{12} in its GGA-PBE version with spin polarization. Filled skutterudites have a crystallographic structure similar to that of binary skutterudites: they crystallize in space group Im3, with Y at 2a (0, 0, 0), Fe at 8c (1/4,1/4,1/4), and P at 24g (0, $y = 0.353$, $z = 0.1501$) positions, respectively [21, 22]. Figure 2 shows the variation of total energy for both non-magnetic (NM) and ferromagnetic (FM) states as a function of volume and lattice constant for YFe_4P_{12} using the Murnaghan equation of state (EOS) [23] to determine the lattice parameter, bulk modulus, and its derivative. It is clear that the most stable structure for the compound YFe_4P_{12} corresponds well to the non-magnetic configuration (NM), or this configuration (NM) always presents the minimum total energy E_0 than the ferromagnetic configuration (FM). The internal parameters y and z, which define the position of the pnictogen atoms, are determined by minimizing the energy while keeping the volume fixed at the experimentally observed value. Table I shows the structural results obtained for the YFe_4P_{12} material. Our calculation of the lattice parameter and bulk modulus of this compound is reasonably in good agreement with the experimental results [14, 22, 24, 25].

3.2. Electronic properties

The energy bands provide the possible energy of an electron as a function of the wave vector. Therefore, these bands are represented in the reciprocal space. Figure 3 shows the structures of the electronic bands according to the directions of

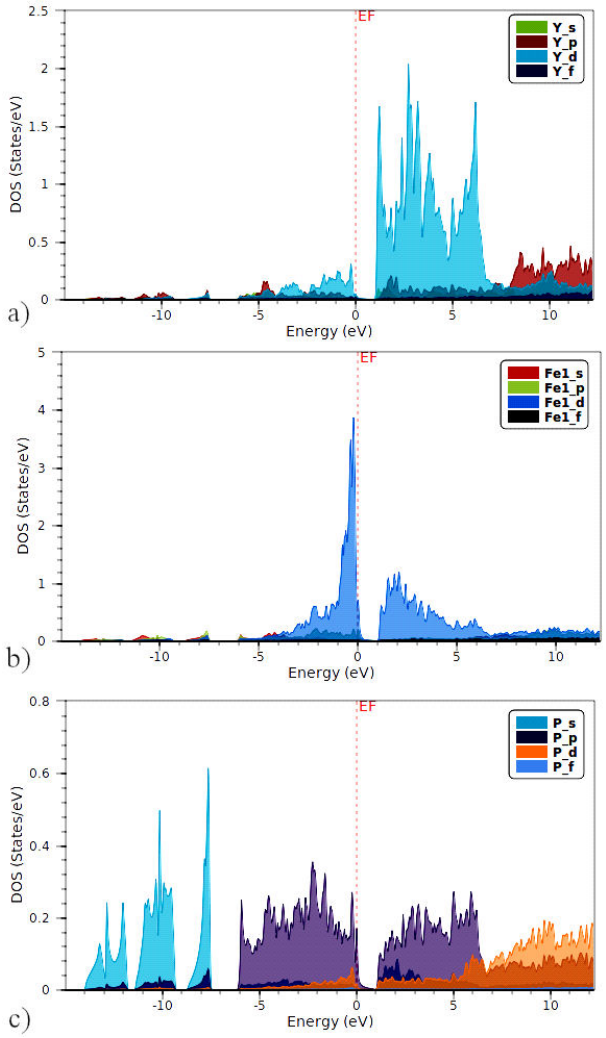

FIGURE 4. The partial density of states of YFe_4P_{12}: at the equilibrium structure using PBE-GGA approximation.

the high symmetry of the Brillouin zone associated with the ground state [20]. The figures are completed with the corresponding partial density of states in Fig. 4 obtained by solving the Kohn-Sham equations using the FP-LAPW method for the compound YFe_4P_{12}. In the case of YFe_4P_{12} alloy, the most important remark is the presence of a metallic character in the majority spins and a semiconductor character with a direct gap $(\Gamma - \Gamma)$ of 0.493 eV in the minority spins, which means that the YFe_4P_{12} alloy is a half-metallic. This means that the non-magnetic YFe_4P_{12} material is not attracted to a permanent magnet. In the case of the YFe_4P_{12} alloy, we note the partial density of states (PDOS) calculated in GGA-PBE. Below the Fermi level, the states are entirely dominated by the Fe-d states, with some contribution from the Y-d, P-s, P-p, and P-d states. Around the Fermi level, the states are dominated by Fe-d and P-p. The states located about 1 eV and more above the level of Fermi come essentially from the states Y-d, Fe-d, P-s, P-p and P-d.

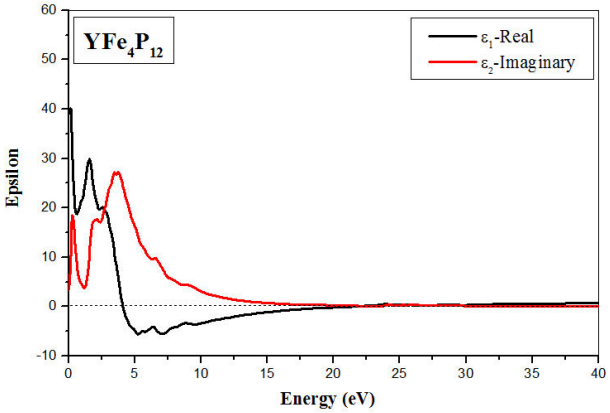

FIGURE 5. The real part $\varepsilon 1(\omega)$ and imaginer part $\varepsilon 2(\omega)$ of dielectric function of YFe_4P_{12}.

3.3. Optical properties

In this part, we discuss the optoelectronic properties of YFe_4P_{12} using first-principles calculations based on the generalized gradient approximation. Characteristics such as the dielectric function, refractive index, reflectivity, optical conductivity, and optical absorption have been reported. The information gathered in this study may be useful in photovoltaic applications. To characterize the linear optical properties of the cubic symmetry YFe_4P_{12} material, it suffices to process a single dielectric tensor component. The dielectric function is considered the most important parameter in linear optics that explains the absorption and polarization properties of materials. The real part of the complex dielectric function ε_1 is plotted in Fig. 5 representing the storage capacity of a material and can be related to polarization. The imaginary part of the dielectric function ε_2 describes the optical adsorption in the crystal and related to the band structure of the material. From Fig. 5, it can be observed that the real and imaginary parts of the dielectric function exhibit almost the same qualitative behavior with some differences in the details. We observed that for smaller frequencies, the curve of the real part has a maximum close to the absorption edge. The decrease in the peak can be explained by interband transitions. Optical absorption in crystals is mainly due to interband transitions, *i.e.* the promotion of electrons from occupied valence bands to empty conduction bands. Regarding the imaginary part, one can note the presence of peaks followed by regions modulated by the peak structures related to the critical points of the Brillouin zone. The main peak of $\varepsilon_1(E)$ is at $E = 0.15$ eV, while that of $\varepsilon_2(E)$ occurs at $E = 3.73$ eV where E is the photon energy. The refractive index (n) is an important fundamental parameter in device design. The calculated $n(E)$ spectrum for YFe_4P_{12} is shown in Fig. 6, which shows the appearance of 6.34 peaks from the excitonic transitions that occur at the edges of $E = 0.15$ eV. Knowledge of the complex dielectric function makes it possible to derive another measurable quantity: the reflectivity spectrum. The results for YFe_44P_{12} are shown in Fig. 7. Note that the maximum of the reflectivity has a value of around 58.7% and is around

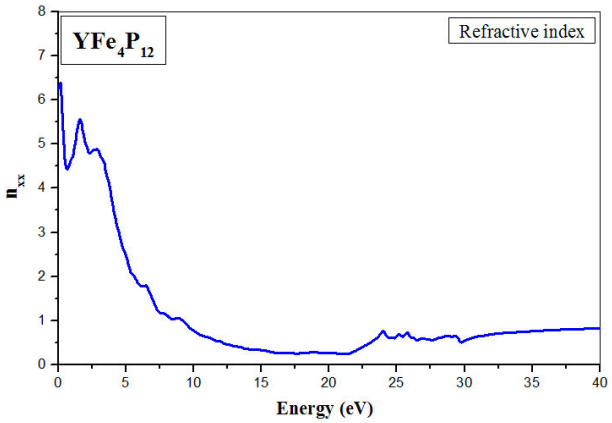

FIGURE 6. The refractive index $n(\omega)$ of YFe_4P_{12} compound.

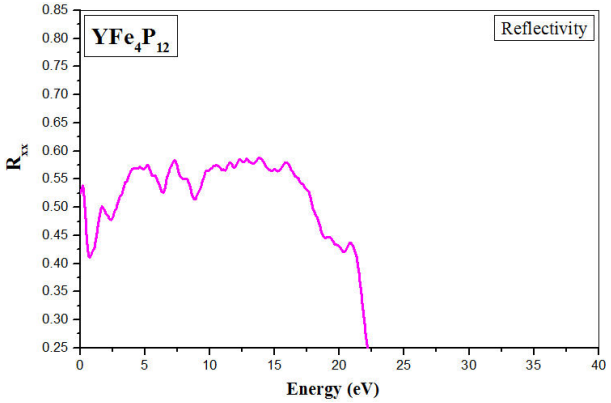

FIGURE 7. The reflectivity $R(\omega)$ of YFe_4P_{12} compound.

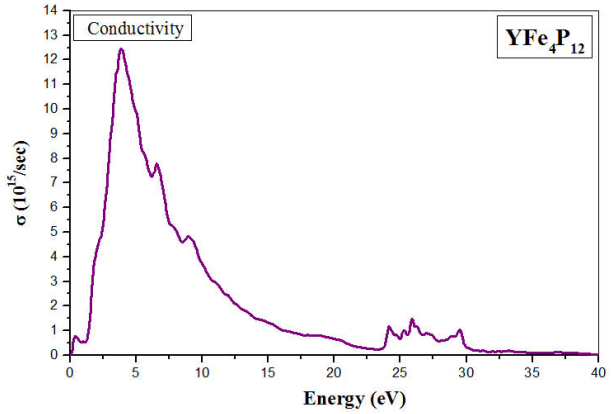

FIGURE 8. The conductivity $\sigma(\omega)$ of YFe_4P_{12} compound.

$\hbar = 13.79$ eV. The peak at this stage is related to interband transitions, which are modified by excitonic effects. Regions characterized by low energy levels exhibit remarkably high reflectivity. This distinctive feature suggests the presence of robust conductance in these particular energy ranges. In other words, the crystal exhibits enhanced reflectivity, meaning its ability to efficiently transmit and reflect light in these low energy ranges, thus indicating strong conductive properties. The optical conductivity spectra of the YFe_4P_{12} alloy as a function of photon energy are shown in Fig. 8. As shown in this figure, the optical conductivity is highly dependent on the photon energy. Its maximum value is reached for photon energy of approximately 3.85 eV. When the photon energy exceeded 40 eV, the optical conductivity disappeared. The occupied states are excited towards the unoccupied states above the Fermi level by the absorption of photons. This inter-band transition is called "optical conductivity" and photon absorption is called "inter-band absorption". Optical conductivity means electrical conduction in the presence of the electric field included in the light. Figure 9 shows the optical absorption coefficient spectrum of YFe_4P_{12}. The penetration of light into a material of a particular wavelength before absorption can be determined using the optical absorption coefficient. The latter was calculated based on the photon energy. Note that the optical absorption coefficient increases with increasing photon energy up to approximately 9.68 eV, then decreases up to approximately 23.54 eV. From a quantitative perspective, the change in the optical absorption coefficient as shown in Fig. 9, depends on the energy of the absorbed light.

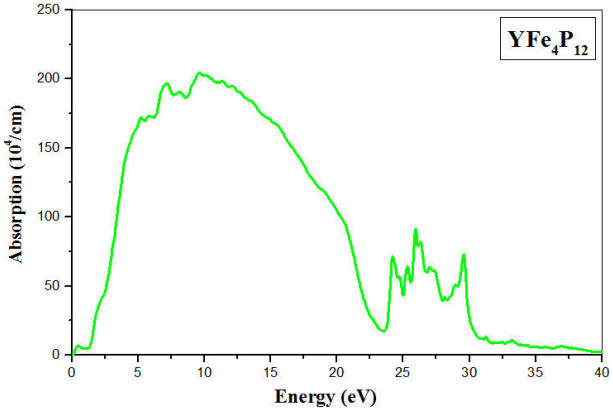

FIGURE 9. The absorption of YFe_4P_{12} compound.

3.4. Thermodynamic properties

Thermodynamics is a science concerned with the relationships that exist within matter between very general properties, such as energy, pressure, or temperature, as well as with how the state of these systems evolves. To study the thermal properties of YFe_4P_{12} at high temperatures and pressures, we applied Debye's quasi-harmonic approximation [26, 27].The quasi-harmonic Debye model allows us to obtain all thermodynamic quantities from the properties of the energies and volumes calculated at equilibrium. In Fig. 10 we present the variation in the lattice parameter as a function of temperature at different pressures for YFe_4P_{12}. When $T < 100$ K, the lattice parameter was almost constant for all applied pressures. When $T > 100$ K, this parameter increases with temperature for a given pressure, whereas when the pressure increases, the crystalline parameter decreases for a given temperature. The growth rate of the lattice parameter with temperature decreased when the pressure was increased. Generally, it is

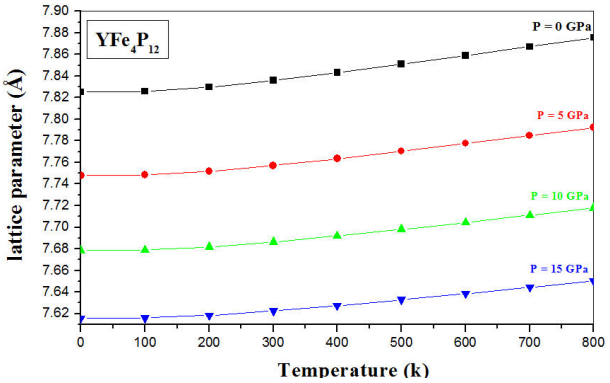

FIGURE 10. The variation of lattice parameter as a function of temperature for YFe_4P_{12} at different pressures.

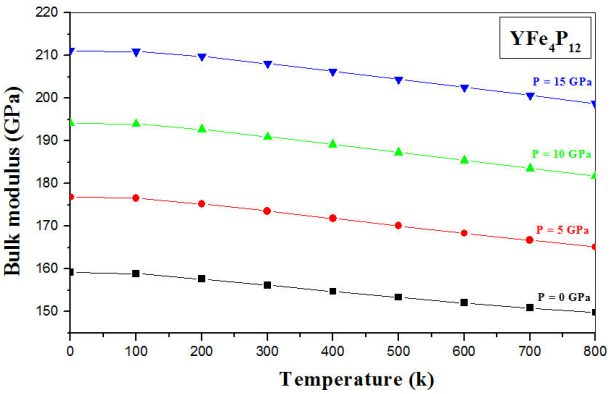

FIGURE 11. The variation of bulk modulus B as a function of temperature for YFe_4P_{12} at different pressures.

noted that the temperature increases the volume of the material; however, the pressure decreases it, from where these opposite effects are observed. It can be noted that the calculated value for the lattice parameter at room temperature and zero pressure is 7.83Å. Figure 11 shows the variation in the bulk modulus as a function of temperature under the effect of pressure. From this figure, we can notice that for a temperature $T < 100$ K, the bulk modulus is constant. This behavior was observed for the lattice parameter, which can be explained by the fact that this temperature range is insufficient to increase the volume of the material and, subsequently, its compressibility. When $T > 100$ K, the compressibility decreases significantly with temperature for a given pressure, indicating that at this temperature, the volume of the YFe_4P_{12} material increases considerably. A rapid change in the volume implies a rapid decrease in the bulk modulus. Decay is important at low pressures. At a given temperature, bulk modulus increases with increasing pressure. Subsequently, the hardness of this material decreases with temperature and increases with pressure. We can conclude that the decrease in temperature and the increase in pressure have similar effects on YFe_4P_{12}. It can be noted that, at $T = 300$ K and zero pressure, the bulk modulus is 156.45 GPa. Knowledge of the heat capacity of a substance not only describes its vibrational properties but is necessary for many applications.

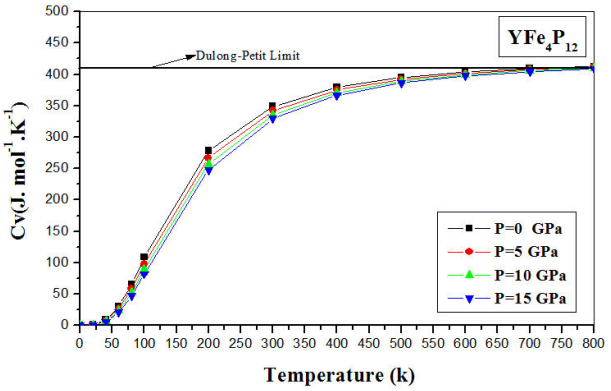

FIGURE 12. The variation of heat capacity C_V as a function of temperature for YFe_4P_{12} at different pressures.

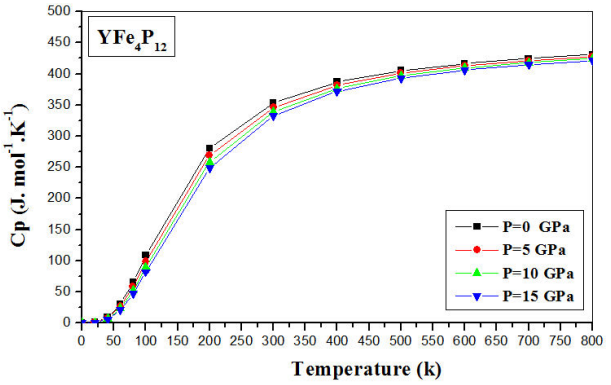

FIGURE 13. The variation of heat capacity C_P as a function of temperature for YFe_4P_{12} at different pressures.

Two well-known limiting cases for this quantity are correctly described by the elasticity theory [27]. At high temperatures, the heat capacity at constant volume C_V does not depend much on temperature and tends towards the Dulong-Petit limit C_V(T)≈ $3R$ for mono-atomic solids [26, 27], which is true for all solids at high temperatures. At sufficiently low temperatures, C_V is proportional to T^3 [27]. The variation in the heat capacity C_V as a function of temperature at pressures ranging from 0 GPa to 15 GPa is shown in Fig. 12. At low temperatures, the heat capacity C_V manifests itself more and more clearly in the direction of increase, *i.e.* it varies proportionally to T^3. However, at high temperatures, the heat capacity at constant volume increases slowly and tends towards the Dulong-Petit limit corresponds to the value of 411.153 J/mol.K. At zero pressure and $T = 300$ K, the value of C_V is 349.6324 J/mol.K. However, we also note that the effect of pressure on the heat capacity C_V is small; for a given temperature the values of C_V for different pressures are very close. The variation in heat capacity at constant pressure C_P as a

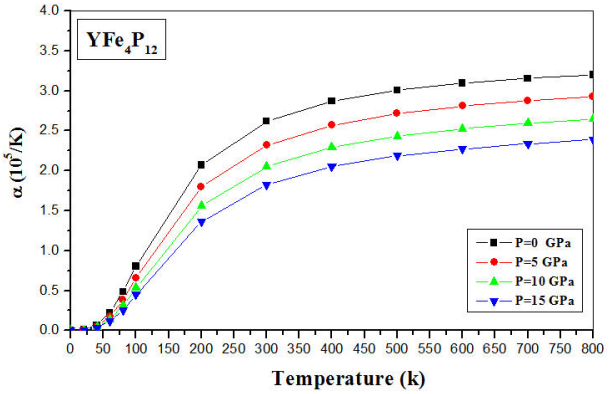

FIGURE 14. The variation of thermal expansion coefficient as a function of temperature for YFe_4P_{12} at different pressures.

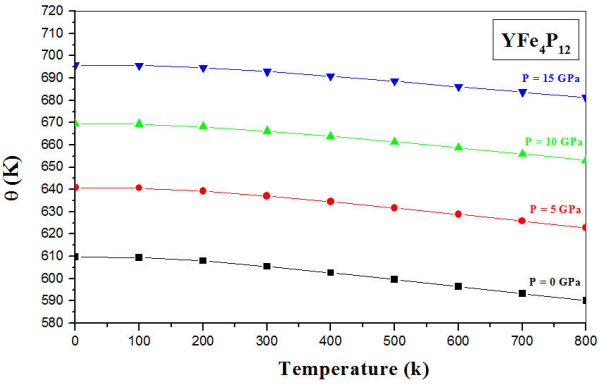

FIGURE 15. The variation of Debye temperature as a function of temperature for YFe_4P_{12} at different pressures.

function of temperature at different pressures for the YFe_4P_{12} alloy is shown in Fig. 13. When the temperature increased, the variations in C_P were similar to those of C_V at low temperatures. At high temperatures, C_P behaves differently than C_V, it does not tend towards a constant value. The effect of pressure on the heat capacity at constant pressure C_P was similar to that of C_V due to its proportionality to the temperature T^3. Thermal expansion is the expansion of the body volume caused by heating. The coefficient of linear thermal expansion is related to the strength of atomic bonds. Strong atomic bonding results in smaller thermal expansion and higher melting points. The variation in the coefficient of thermal expansion as a function of temperature at different pressures for the YFe_4P_{12} compound is shown in Fig. 14. At a given pressure, we can see that the coefficient of thermal expansion increases rapidly with temperature T at lower temperatures (approximately $T < 400$ K), and above this value of 400 K the rate decreases, and the dependence of the coefficient of thermal on temperature is small for high temperatures. Moreover, increasing the pressure decreased the rate of decrease. At zero pressure, the variation of the coefficient in thermal expansion with temperature was greater. Figure 15 shows the evolution of the Debye temperature θ_D with the temperature at several pressures. We see that θ_D is almost constant from 0 to 100 K and decreases linearly when

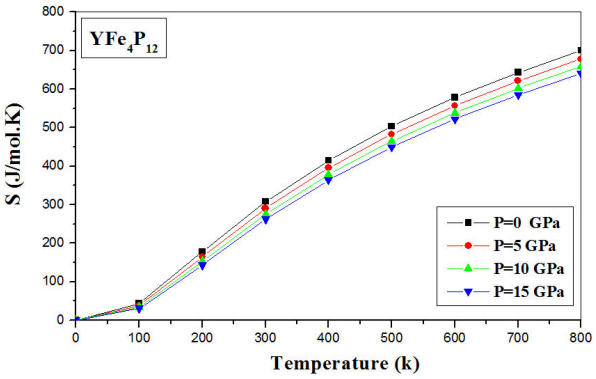

FIGURE 16. The variation of entropy as a function of temperature for YFe_4P_{12}: at different pressures.

the temperature increases. For a fixed temperature, the Debye temperature increases with increasing pressure. By comparing this curve with that in Fig. 11 relating to the bulk modulus, we notice a similar behavior, that is, the Debye temperature and bulk modulus evolve in the same way. Our calculation of θ_D at zero pressure and ambient temperature is equal to 605.77 K. This could indicate that Debye's quasi-harmonic model is a very reasonable alternative to account for thermal effects without a computationally expensive task. Entropy can be interpreted as a measure of the degree of disorder of a system at a microscopic level. The higher the entropy of the system, the fewer its elements are ordered, interrelated, and capable of producing mechanical effects. This can be explained by an increase in the incidence of molecular disorders. The probability of molecules occupying different positions increased. In Fig. 16, we show the variation in entropy S with temperature and pressure for the YFe_4P_{12} alloy. For a given pressure, the entropy S increased sharply with increasing temperature and decreased with increasing pressure at a given temperature. It can be seen in the figure that the entropy S increases rapidly with temperature, and it takes a finite value at low temperatures. Entropy decreases with increasing pressure and increases with temperature. Entropy is more sensitive to temperature and pressure. We notice that the crystal structure is still preserved at 800 K because YFe_4P_{12} alloy was systematically prepared by the reaction of stoichiometric amounts of each metal and red phosphorus powders at pressures between 4 and 5 GPa. The reaction temperatures were between 1000°C (1273.15K) and 1100°C (1373.15 K). These products were characterized by powder X-ray diffraction using CuKa radiation and silicon as a standard at ambient pressure [22].

4. Conclusion

This work aimed at a detailed study of the physical properties of filled Skutterudite YFe_4P_{12} material in its cubic structure using the full-potential and linear augmented plane-wave method (FP-LAPW) based on density functional theory (DFT). This method has proven to be more effective than other calculation methods encountered in solid-state physics.

The generalized gradient approximation (GGA-PBE) was used to determine the exchange and correlation potential. Before studying this material, we investigated the study of its structural properties. We first calculated the ground state properties of compound YFe_4P_{12}, such as lattice constants, bulk modulus, and its derivative. The obtained results were in good agreement with those determined by the available experimental measurements. The results obtained on the band structure showed a metallic character in the majority spins and a semiconductor character with a direct gap $(\Gamma - \Gamma)$ of 0.493eV in the minority spins, which means that the YFe_4P_{12} is a half-metal. The dielectric function, refractive index, reflectivity, optical conductivity, and optical absorption were qualitatively analyzed, and the calculated optical properties revealed a strong response of this material in the energy range between visible light, extreme IR regions, and UV regions, making it a good candidate for optoelectronic applications. The thermal properties were determined in the temperature range of 0-800 K, where the quasi-harmonic model remained fully valid. To the best of our knowledge, comparable experimental results for the optical part are not available, even the temperature and pressure dependence of the lattice parameter. These results ensured the reliability of the current first-principle calculations, so this is a detailed predictive study. It appears that this alloy exhibits a thermodynamically stable behavior and can be developed experimentally.

1. M.S. Torikachvili *et al.,* Low-temperature properties of rare-earth and actinide iron phosphide compounds MFe_4P_{12} (M= La, Pr, Nd, and Th), *Physical Review B* **36** (1987) 8660, https://doi.org/10.1103/PhysRevB.36.8660.
2. E. Bauer *et al.,* Magnetic behaviour of $PrFe_4Sb_{12}$ and $NdFe_4Sb_{12}$ skutterudites, *Physica B: Condensed Matter* **312** (2002) 840, https://doi.org/10.1016/S0921-4526(01)01210-8.
3. G.P. Meisner, Superconductivity and magnetic order in ternary rare earth transition metal phosphides, Physica B+ C **108** (1981) 763, https://doi.org/10.1016/0378-4363(81)90686-0.
4. N. Takeda and M. Ishikawa, The effect of La substitution and magnetic field on non-Fermi-liquid behaviour in $CeRu_4Sb_{12}$, *Journal of Physics: Condensed Matter* **13** (2001) 5971, https://doi.org/10.1088/0953-8984/13/26/312.
5. W. Jeitschko and D. Braun, LaFe4P12 with filled CoAs3-type structure and isotypic lanthanoid-transition metal polyphosphides, *Acta Crystallographica Section B: Structural Crystallography and Crystal Chemistry* **33** (1977) 3401, https://doi.org/10.1107/S056774087701108X.
6. N. T. Stetson, S. M. Kauzlarich, and H. Hope, The synthesis and structure of two filled skutterudite compounds: $BaFe_4Sb_{12}$ and $BaRu_4Sb_{12}$, *Journal of Solid State Chemistry* **91** (1991) 140, https://doi.org/10.1016/0022-4596(91)90067-R.
7. C. B.H. Evers, L. Boonk, and W. Jeitschko, Alkaline Earth Transition Metal Antimonides AT_4Sb_{12} (A= Ca, Sr, Ba; T= Fe, Ru, Os) with $LaFe_4P_{12}$-Structure, *Zeitschrift für anorganische und allgemeine Chemie* **620** (1994) 1028, https://doi.org/10.1002/zaac.19946200613.
8. D.J. Braun and W. Jeitschko, Thorium-containing pnictides with the $LaFe_4P_{12}$ structure, *Journal of the Less Common Metals* **76** (1980) 33, https://doi.org/10.1016/0022-5088(80)90007-7.
9. G.P. Meisner, M.S. Torikachvili, K.N. Yang, M.B. Maple, and R.P. Guertin, UFe_4P_{12} and $CeFe_4P_{12}$: nonmetallic isotypes of superconducting $LaFe_4P_{12}$, *J. Appli. Phys.* **57** (1985) 3073, https://doi.org/10.1063/1.335217.
10. A. Leithe-Jasper *et al.,* Ferromagnetic Ordering in Alkali-Metal Iron Antimonides: $NaFe_4Sb_{12}$ and KFe_4Sb_{12}, *Phys. Rev. Lett.* **91** (2003) 037208, https://doi.org/10.1103/PhysRevLett.91.037208.
11. B.C. Sales, B.C. Chakoumakos, and D. Mandrus, Thermoelectric properties of thallium-filled skutterudites, *Phys. Rev. B* **61** (2000) 2475, https://doi.org/10.1103/PhysRevB.61.2475.
12. B.C. Sales, D.W.R.K. Mandrus, and R. Kifilled Williams, Filled skutterudite antimonides: a new class of thermoelectric materials, *Science* **272** (1996) 1325, https://doi.org/10.1126/science.272.5266.1325.
13. J.-S. Choi, H.-J. Kim, H.-C. Kim, D.-B. Hyun, and T.-S. Oh, presented at the XVI ICT'97. Proceedings ICT'97. 16th International Conference on Thermoelectrics (Cat. No. 97TH8291), 1997 (unpublished).
14. J. Hayashi *et al.,* Bulk Moduli of Superconducting filled skutterudites YT_4P_{12} (T= Fe, Ru and Os). *Photon Factory Activity Report* **2008** # 26 Part B (2009).
15. I. Shirotani *et al.,* Superconductivity of new filled skutterudite YFe_4P_{12} prepared at high pressure, *Journal of Physics: Condensed Matter* **15** (2003) S2201, https://doi.org/10.1088/0953-8984/15/28/352.
16. K. Magishi *et al.,* NMR study of the new filled skutterudite superconductor YFe_4P_{12}, *Physica B: Condensed Matter* **359** (2005) 883, https://doi.org/10.1016/j.physb.2005.01.333.
17. P. Blaha, K. Schwarz, G. K.H. Madsen, D. Kvasnicka, and J. Luitz, wien2k, *An augmented plane wave+ local orbitals program for calculating crystal properties* **60** (2001).
18. A. Ababou *et al.,* DFT-based computer simulation of the physical properties of transparent conducting oxide of delafossite-type: $AgInO_2$ and $AgYO_2$, *Physica B: Condensed Matter* **601** (2021) 412584, https://doi.org/10.1016/j.physb.2020.412584.
19. J. P. Perdew, Kieron Burke, and Matthias Ernzerhof, Generalized gradient approximation made simple, *Phys. rev. lett.* **77** (1996) 3865, https://doi.org/10.1103/PhysRevLett.77.3865.

20. A. Touia, K. Benyahia, and A. Tekin, First-principles calculations of structural, electronic, optical, and thermoelectric properties of LuNiBi and LuNiSb half-heusler, *Journal of Superconductivity and Novel Magnetism* **34** (2021) 2689, https://doi.org/10.1007/s10948-021-05970-3.

21. L. Eyring, K. A. Gschneidner, and G.H. Lander, Handbook on the physics and chemistry of rare earths. (Elsevier, 2002).

22. I. Shirotani, Y. Shimaya, K. Kihou, C. Sekine, and T. Yagi, Systematic high-pressure synthesis of new filled skutterudites with heavy lanthanide, $LnFe_4P_{12}$ (Ln= heavy lanthanide, including Y), *Journal of Solid State Chemistry* **174** (2003) 32, https://doi.org/10.1016/S0022-4596(03)00170-1.

23. M.A. Blanco, E. Francisco, and V. Luana, GIBBS: isothermal-isobaric thermodynamics of solids from energy curves using a quasi-harmonic Debye model, *Computer Physics Communications* **158** (2004) 57, https://doi.org/10.1016/j.comphy.2003.12.001.

24. J. Hayashi *et al.*, X-ray diffraction study of filled skutterudite superconductors at high pressures, Photon Factory Activity Report **2007** #25 Part B (2008).

25. J.-G. Cheng *et al.*, Pressure dependence of the superconducting transition temperature of the filled skutterudite YFe_4P_{12}, *Phys. Rev. B* **88** (2013) 024514, https://doi.org/10.1103/PhysRevB.88.024514.

26. A. Touia, M. Ameri, and I. Ameri, Synthesis, crystal structure and physical properties of the thulium filled skutterudite $TmFe_4P_{12}$ under the effect of the pressure: LDA and LSDA calculation, *Optik* **126** (2015) 3253, https://doi.org/10.1016/j.ijleo.2015.07.130.

27. I.R. Shein, K.I. Shein, N.I. Medvedeva, and A.L. Ivanovskii, Electronic properties of $ThSiO_4$ polymorphs (thorite and huttonite) from first principles calculations, *physica status solidi (b)* **243** (2006) R44, https://doi.org/10.1002/pssb.200642093.